Chiral oscillations in electronic transport through graphene nanoribbons induced by pseudospin filters

Luis I. A. López [*]
Faculdade de Ciências Exatas - IEA, Universidade Federal do Sul e Sudeste do Pará, CEP 68560-000, Santana do Araguaia, Pará, Brazil

Michel Mendoza [†]
Centro de Ciências Naturais e Humanas, Universidade Federal do ABC, 09210-170, Santo André, São Paulo, Brazil

(Received 7 November 2019; revised 12 March 2020; accepted 19 October 2020; published 4 November 2020)

We show here that the application of potential barriers that induce contributions of hyperboloid subbands (pseudospin filters) in graphene nanoribbons locally breaks the chiral symmetry of the Dirac state, in the sides of the barrier, with the consequent transition from Klein to anti-Klein behavior. With the increased filter potential applied, resonances of Fabry-Pérot type with line widths that are decreasing are generated in the conductance, which is associated with a pseudospin precession located on the sides of the barrier. Interestingly, throughout this process the chiral symmetry of the state is conserved, and pseudospin oscillations (opposite) that increase in intensity are observed on the sides of the filter. This is associated with a gradual loss of the electron-hole correlation, with the increased filter potential, which ends with the formation of a transport gap when the electron-hole symmetry is completely broken. This is an example of how the chiral symmetry can evolve and still be conserved, during a tunneling process. All this leads to the generation of energy gaps, associated with anti-Klein tunneling, which can be controlled using certain spatial configurations of the applied filters. The inclusion of a new type of asymmetry (roughness in the filters) makes it possible to recover Klein's tunneling in the region of induced gaps. The interaction of the hyperboloid subbands with the Dirac band can be observed in density-of-states maps using the pseudospin filters, following the behavior of the van Hove singularities as a function of the filter potential.

DOI: 10.1103/PhysRevB.102.205404

I. INTRODUCTION

Chirality in graphene is a geometric property, associated with the existence of an object and its mirror image (left- and right-handed counterparts) coexisting together, which are intrinsically correlated. Thus the chiral property has two important characteristics: symmetry and correlation.

In graphene these counterparts are the sublattices A and B. This chiral property of the lattice is transmitted for the states of the system when we model these as a linear combination of the atomic sites of the sublattices A and B [1,2]. In this way, the state vector will have two components, called pseudospins [3], and each pseudospin is associated with a single sublattice. In the natural case (undisturbed graphene) the two sublattices contribute in the same way, which is called chiral symmetry. Thus, the symmetry observed between the two components (pseudospins) of the state vector is a consequence of the chiral property of the graphene lattice. An external disturbance can break the chiral symmetry, leading to changes in the components of the state vector, which generates a relative pseudospin polarization (the state becomes more polarized in a sublattice). For example, by applying a different potential to the two sublattices, the chiral symmetry can be lifted. This can be done by aligning the flake on a hexagonal boron nitride substrate [4,5]. The closely similar lattice structures of graphene and hexagonal boron nitride result in local alignment of the atomic site A of graphene with a boron atom and its B site with a nitrogen atom (or vice versa). In this situation, the two carbon sites therefore experience different potentials, leading to the broken chiral symmetry, generating energy gaps associated with anti-Klein tunneling, which is understood in terms of lack of pseudospin matching.

In general, the two components of pseudospin are related to each other, when one component increases, the other decreases. For this reason, one way of measuring the chirality property is directly related to the relative phase between the two components of pseudospin (correlation). In this way, an increase in the polarization of pseudospin means an increase in the loss of chiral symmetry.

Chiral materials, such as graphene, possess left- and right-handed counterparts linked by mirror symmetry. These materials are useful for advanced applications in polarization optics [6,7], stereochemistry [8,9], and spintronics [10,11]. For example, if we pass a polarized light through a chiral crystal, the polarization is maintained. On the other hand, if we disturb the chiral crystal in such a way as to break the chiral symmetry (nonhomogeneous contribution of the counterparts), two new polarizations will be observed, which are associated with the left- and right-handed counterparts. In this way, using these ideas in bilayer graphene, a chiral

[*] luis.lopez@unifesspa.edu.br
[†] michel.mendoza@ufabc.edu.br

stacking approach was reported, wherein two-dimensional materials are positioned layer by layer with precise control of the interlayer rotation and polarity, resulting in tunable chiral properties of the final stack [12].

Chirality is determined by the relative phase in the two-component wave function of the Dirac quasiparticle (correlation between pseudospins), which arises from the sublattice composition in graphene [13]. The phase shift in the sublattice composition of the electron states in graphene has been detectable by angle-resolved photoemission spectroscopy [14–17]. An alternative technique for pseudospin and chirality detection is based on tunneling of electrons in van der Waals heterostructures in which graphene and hexagonal boron nitride are stacked in a multilayer structure. In that work, it is shown that the tunneling current-voltage characteristics, in the presence of an in-plane magnetic field, essentially depend on the pseudospin orientation and enable detection of the valley sublattice structure determined by the relative phase between the two sublattice components of the Dirac spinor vector wave function of electrons in graphene. For the case of chiral electrons, different states in momentum space (and thus with specific pseudospin orientation) have different tunneling probability, depending on whether the interference between the two components of electron wave function is constructive or destructive as electrons tunnel out of the emitting graphene layer [13].

In general, the chiral symmetry of the graphene lattice generates the electron-hole state or Dirac state (around the Dirac point), which was previously called the state vector. A breakdown of chiral symmetry leads to a breakdown of the electron-hole correlation. This correlation is related to the correlation that exists between the pseudospins, the latter being directly related to the correlation that exists between the sublattices of graphene.

For the case of chiral symmetry, the Dirac state is a solution of the Dirac equation for massless fermions. The chiral symmetry or conservation of pseudospin (polarization of pseudospin zero) leads to the absence of backscattering and to Klein tunneling, in which the barrier behaves as transparent. Thus, the chiral properties of Dirac electrons in monolayer graphene have been used to explain Klein tunneling and the absence of backscattering in graphene p-n junctions [18–22]. On the other hand, if the Dirac fermion acquires mass (because of the breakdown of chiral symmetry), a mass term is necessary in the Dirac Hamiltonian, generating pseudospin polarizations, and opens an energy gap around the Dirac point, as happens in bilayer graphene [23–27]. In this way, the mass signifies a break of the chiral symmetry and a component of the pseudospin vector, perpendicular to the graphene plane, is induced [28]. Also in bilayer graphene, signatures of the broken chirality due to band gap opening should be accessible in experiments as Fabry-Pérot resonances [28–30].

Klein tunneling in graphene is a holonomic adiabatic cyclic process, and for massless Dirac fermions it has an associated Berry phase of π [31–37]; this phase characterizes the chiral symmetry or polarization of pseudospin zero. Acquiring a Berry phase of π means the inversion of the pseudospin components of the state vector, thus conserving the chiral symmetry.

On the other hand, it would be expected that, for the breakdown of chiral symmetry (polarization of pseudospin different from zero) due to the mass term in the Hamiltonian of holonomic processes, the Berry phase is different from π. This for example is observed in bilayer graphene, and when disorder or impurities exist the Berry phase becomes a function of the disorder (asymmetry) [28]. In general, changes in chiral asymmetry of state lead to changes in the associated Berry phase. This is why the Berry phase is often called the pseudospin winding number [38]. This integer number represents the degree of chirality [39].

Chirality also exists in the lattice of metallic armchair graphene nanoribbon (metallic-AGNR), therefore the effects discussed above can also be observed in these nanoribbons. On the other hand, edge effects and topological states are also observed in nanoribbons [34,40–42]. Here in our work, we study a metallic-AGNR disturbed by a potential barrier (pseudospin filter) [3,43–47] and we discuss the tunneling process based on the characteristics of the applied barrier: height V and width L_b.

One of our main results is the nonmonotonic behavior of the conductance $G(V)$, with Fabri-Pérot resonances that decrease its line width as V increases, until a transport gap is generated. In general, our system presents quantum confinement in the region of the applied barrier. The state associated with the tunneling process (for energies around the Dirac point) always has a special shape. Where pseudospin polarizations are observed on the sides of the barrier, then we have partial polarizations on the sides [PP(V)] [3,43–47]. Interestingly, the pseudospin on the right side is always opposite to the one on the left, with a phase of π always between them. This always happens, even as the PP(V) oscillates and increases on each side of the barrier as V increases. As a consequence, the state's pseudospin polarization (which extends throughout space) is always zero, even though there are local polarizations (on the sides of the barrier) that are changing. Therefore, as long as there is tunneling, we have chiral symmetry conservation, even though we do not have chiral symmetry on the sides of the barrier. This is an example of how the chiral symmetry can evolve and still be conserved. The PP(V) oscillations observed in our system are associated with chiral oscillations.

In general, quantum electrodynamics and Gauge theory predict chiral oscillations in a situation of quantum confinement, which alters the effects of quantum interference that can arise in the system [48–50]. On the other hand, Klein tunneling for graphene, widely explained in the literature, does not present chiral oscillations (there are no local polarizations of pseudospin) and there is no quantum confinement; for this reason, only the chiral operator (without the use of a more formal theory of quantum interference) is sufficient to explain that process.

The Fabri-Pérot resonances [observed in $G(V)$] that decrease in line width as V increases, are associated with the gradual loss of correlation between the components of the state, associated with the correlation between the pseudospins. In general, during the process of formation of the transport gap as a function of V, the chiral asymmetry on the sides of the barrier increases [PP(V) increases periodically], which leads to the gradual breakdown of the electron-hole correlation.

When the transport gap is formed, two totally uncoupled states are formed on the sides of the barrier, which have opposite pseudospins. This would be associated with the total loss of correlation between the pseudospins. In this way, the decrease in the line widths, observed in $G(V)$, would be associated with the decoupling of the hole-type wave inside the barrier with the electron-type waves outside the barrier or gradual breakdown of the electron-hole correlation.

Our results do not change as a function of the width W of the nanoribbon. Our results only depend on the characteristics of the barrier: V and L_b. On the other hand, we show here that the imperfections both in the armchair edge of the ribbon as well as in the bulk do not change the Fabri-Pérot resonances; $G(V)$ is practically unaltered. This is totally different from the case when we affect the coupling region between the external and internal parts of the barrier, where the destruction of $G(V)$ is evident. In general, we can conclude that the region of the barrier (especially the interfaces) with characteristics V and L_b is the main cause of the effects observed.

We show here that hyperboloid subbands can reach the Dirac point ($E = 0$) for high potentials V of the applied barrier, consequently the Dirac band will be disturbed in the barrier region. This changes the characteristics of the bands within the barrier region, and for this reason the nanoribbon-barrier interfaces control the tunneling. These interfaces control electron-hole coupling, which is decreasing with increasing V, due to chiral asymmetry in those regions (on the sides of the barrier). In general, the hyperboloid subbands that reach the Dirac point (induced by the chiral disturbance generated by the barrier) are causing the quantum confinement observed in the system. The displacement of the hyperboloid subbands for the Dirac point is evident, where clearly the van Hove singularities of the DOS (which are found where a hyperboloid subband begins) are closer to the point $E = 0$ as V increases.

In this way we use DOS(V, E) to map as the energy bottom (conduction) and energy top (valence) of the hyperboloid subbands (closer to the Dirac point) arrive at the Dirac point; this is done following the behavior of the van Hove singularities. In these maps we can see how the system energies change as a function of V. These maps show the disturbed energies $E(V)$. On the other hand, these maps allow us to deduce that the hyperboloid subbands (seen here as van Hove singularities: bottom and top of the hyperboloid subbands closest to the Dirac point) arrive at the Dirac point, touch, and then move away from that point.

Finally, here in our work we also discuss how we can induce all these effects for low V potentials of the applied filter.

II. THE CALCULATION METHOD

In this work we consider systems composed of one metallic armchair graphene nanoribbon of width W, perturbed by potential barriers of height V and width L_b, Fig. 1(a). Here, we considered systems with widths between $W = 6$ nm (graphene nanoribbon) and $W = 40$ nm (graphene ribbon) [51].

Our simulations are based on the Green function tight-binding formalism [52], where the first neighbors interaction

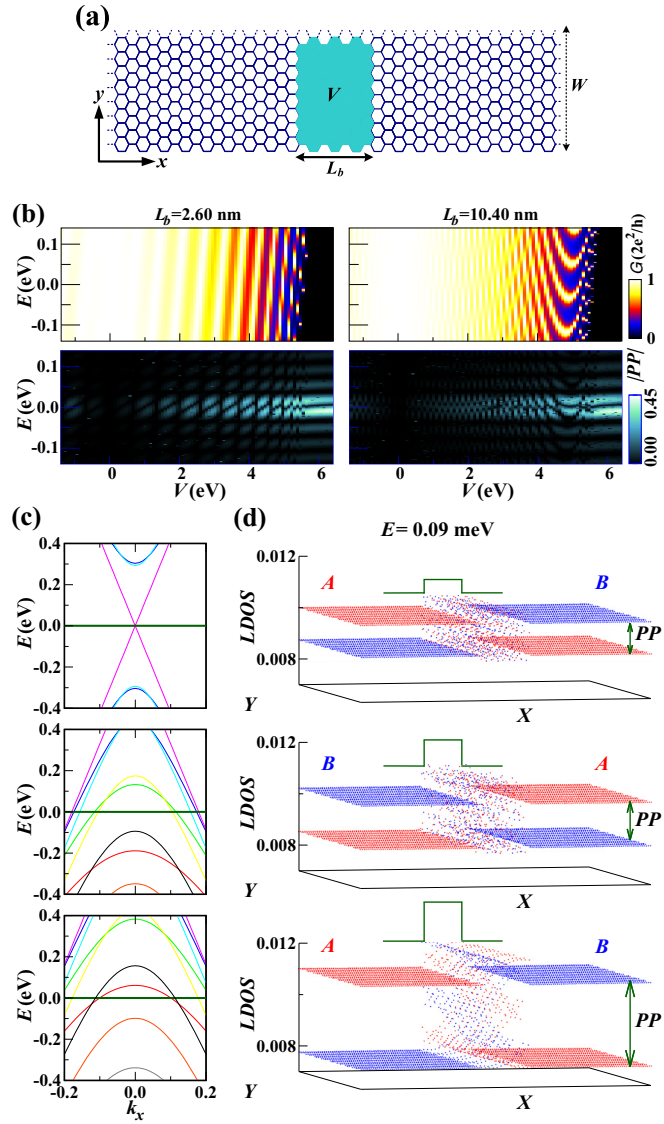

FIG. 1. (a) Metallic armchair graphene nanoribbon with an applied pseudospin filter of potential V (eV). (b) Conductance maps and partial pseudospin polarization maps, for two widths L_b of the applied filter. (c) Energy bands within the applied pseudospin filter region for some potential barrier energies V [0.0 (upper), 0.8 (central), and 1.0 (lower)]. (d) Local density of states, showing the partial pseudospin polarization at both sides of the applied filter.

Hamiltonian can be written as

$$H = -\sum_{i,j} t|i\rangle\langle j| + \sum_{j} V(j)|j\rangle\langle j|. \tag{1}$$

The hopping energy [14] t is approximately 3 eV and $V(j) = V$ is the electrostatic potential that acts on the graphene nanoribbons sites along L_b. We used this tight-binding Hamiltonian to built a bricklayer lattice [53,54], topologically equivalent to a graphene lattice with sites $i = (x, y)$.

The retarded Green propagators are calculated by

$$g(E) = (E - H - \Sigma^L - \Sigma^R + i0^+)^{-1}, \tag{2}$$

where the self-energies [55] Σ^R (right) and Σ^L (left) of the contact leads are numerically calculated using the recursive

Green function method [52,56,57], and H defines a central region that does not consider the contact leads' Hamiltonians, H_R and H_L [all assembled via Eq. (1)]. Using the above definitions we can write $\Sigma^{R(L)} = \tau^{\dagger}_{R(L)} g_{R(L)} \tau_{R(L)}$, where $g_{R(L)}(E) = (E - H_{R(L)})^{-1}$ and $\tau_{R(L)}$ represent the couplings between H and $H_{R(L)}$ respectively. The propagators $g_{R(L)}(E)$ are calculated recursively.

Using the Green propagators $g(E)$ we calculate the local density of states (LDOS) as

$$\rho_E(x, y) = -\frac{1}{\pi} \mathrm{Im}[g(E, x, y)], \tag{3}$$

where the LDOS is defined for each site $i = (x, y)$ of the lattice. Here, we used the LDOS to visualize the partial pseudospin polarizations induced at both sides of the applied barriers.

Using the LDOS the partial pseudospin polarization PP(E) can be obtained by

$$\mathrm{PP}(E) = \frac{\sum_i \rho_{E,A} - \sum_i \rho_{E,B}}{\sum_i \rho_E}. \tag{4}$$

The partial pseudospin polarization is defined for a given energy E using the sites i of the system, where the A (B) subscript corresponds to the use of only A (B) sites in the calculations. In this work we are interested in the partial pseudospin polarization at each side of the applied barrier, which is nonzero. For this reason, throughout the work the PP is defined using only the sites on one side of the barrier, which defines a partial polarization.

On the other hand, the expression for the density of states (DOS) is written as

$$\mathrm{DOS}(E) = -\frac{1}{\pi} \mathrm{Im}\{\mathrm{Tr}[g(E)]\}. \tag{5}$$

Finally, the conductance is obtained by the Fisher-Lee relation [58]

$$G(E) = \frac{2e^2}{h} \mathrm{Tr}[\Gamma_L g(E) \Gamma_R g^{\dagger}(E)], \tag{6}$$

where $\Gamma_{L(R)} = i[\Sigma^{L(R)} - (\Sigma^{L(R)})^{\dagger}]$.

To illustrate what occurs within the applied barrier region, we can use the method described in Ref. [59] to find the dispersion relation of the π electrons. In general, this method reproduces very well the Dirac cone around $E = 0$ and the hyperboloid subbands for energies far from zero [see $E(k_x)$ for $V = 0$, Fig. 1(c)]. We considered potential barriers with several widths L_b and energies V up to 6 eV for illustration. To simulate realistic cases, we have also considered large values for the nanoribbon width W. This is done in order to move the hyperboloid subbands close to the Dirac point (in the system without applied barrier), and thus to be able to use potentials barriers between 1 and 2 eV, which are the ones usually considered in experiments. It is interesting to mention here that a similar effect is achieved when interactions of seconds and third neighbors are included in the tight-binding method [60].

Another interesting effect of the increase in W is that the number of resonances observed does not change to energies around the Dirac point, because the number of oscillations depends only on the L_b of the applied barrier. For this reason, to be able to perform a systematic study of the decrease in line widths depending on the applied barrier, we use throughout the paper the smallest W possible ($W = 6.2$ nm); with that we also save computational time. In general, the effects studied here in this work do not depend on W.

Finally, throughout the work we will discuss other conditions that can diminish the potentials used, to see the effects studied here, in order to encourage future experimental work.

III. RESULTS AND DISCUSSION

In this part of the work, we will first discuss the main effects generated by the application of a potential barrier which induce contributions from the hyperboloid subbands (pseudospin filter), on a metallic armchair graphene nanoribbon, Fig. 1(a). The width of the nanoribbon is W and the characteristics of the applied filter are potential V and width L_b.

The effects produced in the conductance G due to the application of the pseudospin filter are shown in Fig. 1(b). The conductance based on the incident energy of the carriers, E, and the applied potential, V, in the filter, are shown in the upper panels for two values of L_b of the filter. In general, on these maps $G(V, E)$ we see three regimes of transport. For low potential V (little contribution from hyperboloid subband), we have a pure Dirac regime, where Klein's tunneling is perfect. For intermediary V values (appreciable contribution of the hyperboloid subband), minima arise between the maximum of transmission ($T = 1$), and are getting deeper and deeper with the increase of V. These minima are associated with a gradual evolution of an anti-Klein tunneling for normal incidence, similar to what happens in the case of bilayer graphene [28,61]. This intermediate transport regime is characterized by Fabry-Pérot resonances in conductance; note the dependence of the resonances as a function of width L_b of the applied filter. Finally, we arrive in a regime where the formation of a transport gap is observed, for a strong contribution of the hyperboloid subband (high V).

Simultaneously, changes in the partial pseudospin polarization (PP, defined only on one side of the barrier) are observed on the sides of the applied filter, with clear fingerprints observed in this PP associated with the three transport regimes discussed above; see lower panels of Fig. 1(b). Here, we see that Klein's pure regime is associated with very low partial polarizations, with PP going to zero when V goes to zero. The intermediary regime shows a PP that oscillates and increases in intensity with the increase of V. Finally, the transport gap regime is associated with a PP of greater intensity and that does not present oscillations. All these effects are well appreciated around the Dirac point ($E \approx 0$).

In Fig. 1(c) we show qualitatively that the increase in potential V drives the hyperboloid subbands up to the Dirac point. In this situation, the transport of the quasi-particles would be associated with bands that would be a combination of the Dirac band with the hyperboloid subbands. To calculate the energy dispersion relation we have used the method described in Ref. [59]. The contributions of the potential barrier V were added to the dispersion relation as energy of the site; i.e., V is applied on whole graphene nanoribbon. This method aims to show what happens when a potential is applied to

the metallic armchair graphene nanoribbon; in that model the boundary conditions are not of interest, and the barrier can be understood as having an infinite width. In any case, this method is useful to illustrate that hyperboloid subbands can contribute, within the region of the barrier, to the properties of electronic transport using high potentials. In the final part of our work, we will show a technique for qualitatively mapping the contribution of hyperboloid subbands in the system, which takes into account all the characteristics of the pseudospin filter.

The main effect produced by the pseudospin filter is the generation of a polarization of pseudospin on the sides of the filter, PP; see Fig. 1(d). A polarization A or B in a region of space (x, y) induces a spatial asymmetry, because of the imbalance between the contributions of sites A and B for local densities. This PP induced by the V increase, associated with the contribution of the hyperboloid subband in the region of the applied filter, has opposite polarizations at both sides of the filter, which can be reversed for certain values of V. In general, the existence of an opposite PP at both sides of the filter induces an extra asymmetry in the transport direction (x axis), which increases with the increase of V.

It is important to mention here that the use of $n = 1, 2, 3, 4, \ldots$ sites to form L_b always generates polarizations on the sides of the barrier that are opposite. That is, the fact of these polarizations are opposite does not depend on L_b. On the other hand, the nanoribbon-barrier interfaces are always zigzag, which may be favoring the formation of topological states [34,40–42] on the sides of the barrier to preserve chiral symmetry during the tunneling process.

The state associated with the tunneling process (for energies around the Dirac point) always has the shape as shown in Fig. 1(d). Where pseudospin polarizations are observed on the sides of the barrier, then we have partial polarizations on the sides [PP(V)]. Interestingly, the pseudospin on the right side is always opposite to the one on the left, with a phase of π always between them. This always happens, even as the PP(V) oscillates and increases on each side of the barrier, as shown in Fig. 2. In that figure, the blue and red curves are the relative PP(V) for each pseudospin on one side of the barrier [for the other side of the barrier, the blue and red curves are interchanged; see Fig. 1(d)]. As a consequence, the state's pseudospin polarization (which extends throughout space) is always zero, even though there are local polarizations (on the sides of the barrier) that are changing. Therefore, as long as there is tunneling, we have chiral symmetry conservation, just as we do not have chiral symmetry on the sides of the barrier. All this is possible because of the correlation that exists between the sides of the barrier, for the state vector. When this correlation disappears, the sides of the barrier are disconnected, leading to the formation of the transport gap (localization of the state). In general, in Fig. 2 we are observing a process, as a function of V, of the chiral symmetry breaking in the system, which has an adiabatic character (the system changes while preserving chiral symmetry), maintaining the Berry phase of π during whole the process (as a function of V).

The hole-type wave inside the region of the filter is coupled with the pseudospin on the sides of the filter (associated with the electron-type wave), and this coupling is controlled by the

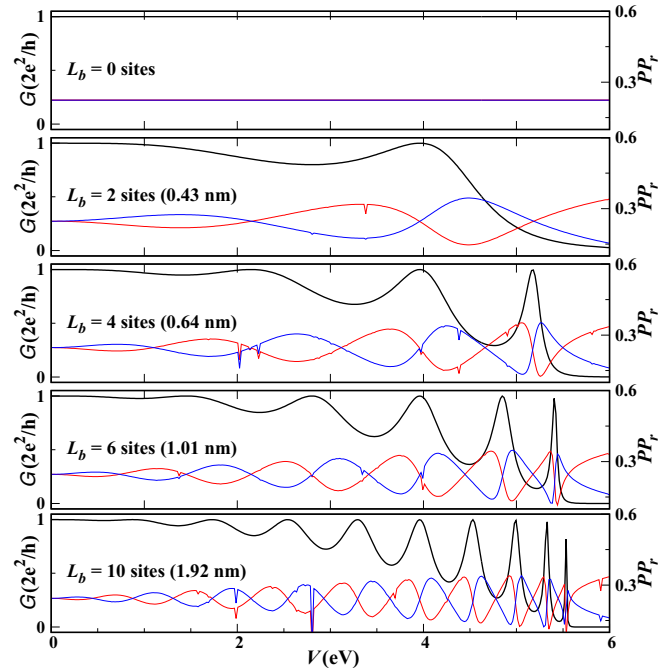

FIG. 2. Conductance G depending on the voltage V of the applied filter, for different widths L_b of the filter (black curve), for $E \approx 0$. The polarizations of pseudospin A (red curve) and B (blue curve), induced by the filter, are also shown. The $G(V)$ shows a nonmonotonic behavior associated with the loss of the property of chirality as V increases.

applied potential V; see Fig. 1(d). The asymmetry induced in the system due to the increase in the intensity of the PP favors the decoupling between the electron wave and the hole wave, or the loss of chirality [4,5,28]. To verify this we use Fig. 2, where the conductance as a function of V, $G(V)$, is studied.

In Fig. 2, we show that the conductance $G(V)$ (for $E \approx 0$), the black curve, shows oscillations. In general, the $G(V)$ in our work shows a transition from a Dirac type limit, represented by Klein tunneling, to a disturbed Dirac limit, represented by oscillations of $G(V)$ and PP(V), with the final generation of Klein antitunneling, associated with the formation of a transport gap. All this is associated with the contribution of the hyperboloid subband as the potential V of the filter increases. The $G(V)$ shows resonances of Fabry-Pérot type, whose line widths decrease with the increase of V, until this width becomes zero and the transport gap is formed. We also observe here that the number of resonances depends on the number of sites used to define the width of the filter (L_b). For large values of L_b all the effects mentioned here are better defined.

On the other hand, as shown in the figure, the polarization of the sublattice A (red curve) oscillates, alternating with the polarization of the sublattice B (blue curve). This would be the analog of the oscillations of spin up and spin down reported for systems with spin precession. Here, the pseudospin polarization happens at both sides of the applied filter [see Fig. 1(d)], so we can infer that the state with contributions only of the sublattice A comes in and the state with contributions only of the sublattice B comes out, which is why we call this partial pseudospin polarization (PP). For this reason the red and blue curves were calculated to the left side of

the filter (the region without an applied barrier) or the input conductance region. In general, we observe that the PP to the left of the filter is periodically inverted as a function of V.

For Fig. 2, a relative PP (PP_r) was used for sublattice A (red curve) and another for sublattice B (blue curve), in order to see the role of each sublattice. The PP_r for sublattice A is calculated using Eq. (4) without considering the contributions of sublattice B. Similarly we calculate the PP_r of sublattice B without considering the contributions of sublattice A. The PP_r have the same information as the PP, but with the advantage that they show the contributions of sublattices A and B separately. In general, the difference between these two PP_r retrieves the PP defined in Eq. (4).

We observe here that for certain values of V a partial polarization (PP) A or B is associated with the conductance, and that this PP increases with the increase of V (watch the red and blue curves move away more and more periodically). In general, the hole-type wave within the region of the barrier is modulated by the width L_b of the filter. This modulation manipulates the coupling of the pseudospin (at both sides of the filter) with the hole-type wave, which is manifested in the conductance as resonances of Fabry-Pérot type that depend on L_b (black curve). Here, the number of resonances is equal to the number of sites occupied by L_b.

As mentioned before, chiral symmetry conservation means, for the Klein tunneling, gaining a Berry phase of π during the process, that is, inverting the pseudospin components of the state. As explained here, in the whole tunneling process (around the Dirac point as a function of V), as shown in Fig. 2, we have the conservation of chiral symmetry, that is, the Berry phase of π does not change, except in the presence of disorder in the nanoribbon-barrier interfaces; how this occurs will be discussed later. In general, throughout the tunneling process (for all V), the state has the shape as shown in Fig. 1(d), even as the PP(V) oscillates and increases on each side of the barrier as V increases (Fig. 2). The state's pseudospin polarization is always zero, even though there are local polarizations that are changing. Therefore, we have chiral symmetry conservation, even though we do not have chiral symmetry on the sides of the barrier. This is an example of how the chiral symmetry can evolve and still be conserved. The PP(V) oscillations observed in our system are associated with chiral oscillations.

The Berry phase (ϕ_{Berry}) is half the solid angle subtended by the pseudospin during its motion on the Bloch sphere [28]. The polarization vector of pseudospin in that representation (spherical coordinates) would have the components $P_x = \sin\theta\cos\phi$, $P_y = \sin\theta\sin\phi$, and $P_z = \cos\theta$ (with polar angle θ and azimuthal angle ϕ). On the other hand, $\phi_{\text{Berry}} = \pi(1 - \cos\theta)$. The condition for the tunneling of Klein [transmission $T(V) = 1$] is $\phi_{\text{Berry}} = \pi$, therefore $\theta = \pi/2$ and the components would be now $P_x = \cos\phi$, $P_y = \sin\phi$, and $P_z = 0$, that is, the vector of pseudospin is in the x-y plane (nanoribbon plane). Out of this condition, there would be a P_z component other than zero, and for the extreme case of $\theta = 0$ only the P_z component would exist [anti-Klein tunneling or $T(V) = 0$]; in this case an energy gap is generated. All these characteristics mentioned before, discussed a lot in graphene, can be extrapolated for the metallic armchair graphene nanoribbons, studied here, for energies close to the Dirac point [34,40–42].

The increase in the PP with the increase of V, together with the evolution of anti-Klein tunneling [detected as a decrease in line widths of Fabry-Pérot resonances in the $G(V)$], lead us to interpret that an increase of lack of pseudospin matching is happening between the filter region and at both sides of the filter (loss of the existing correlation in the chiral property [4,5,28]). As we find in the case of chiral symmetry conservation, as discussed before, mass effects and pseudospin component perpendicular to the plane do not exist here in this case. For our case, a decoupling of the state between the internal and external parts of the barrier is happening, caused by a quantum confinement in the barrier region. In general, the increase in the lack of pseudospin matching is related to an increase in the loss of correlation between state pseudospins. The gradual loss of this correlation means the gradual loss of the electron-hole correlation of the Dirac state.

Thus, during the process shown in Fig. 2 (as a function of V) a decrease in the correlation between the components of the Dirac state is happening. This is related to the line shape observed in $G(V)$. In general, the interference process (associated with tunneling) that couples the internal part of the barrier with the external ones defines a line width for the tunneling peak. It is known that when the line width of the tunneling peak decreases, it is because the coupling between the parts is decreasing. In this way, the decrease in the line widths, observed in $G(V)$, would be associated with the decoupling of the hole-type wave inside the barrier with the electron-type waves outside the barrier. This is associated with the loss of correlation between the components of the state, associated with the correlation between the pseudospins, which are associated with the A and B sublattices that maintain the chirality of the system. In general, during the process of formation of the transport gap as a function of V, the chiral asymmetry on the sides of the barrier increases [PP(V) increase]. When the transport gap is formed, two totally uncoupled states are formed on the sides of the barrier [see Fig. 3(a), lower left], which have opposite pseudospins. This would be associated with the total loss of correlation between the pseudospins.

In Fig. 3(c), for $E = 0$, it is observed that the conductance as a function of L_b, $G(L_b)$, has a frequency that remains constant for a given V; when V changes to another value it is observed that the frequency in $G(L_b)$ also changes, but it remains constant in the function of L_b. That is, for the same asymmetry (PP) the resonance conditions are periodic as a function of L_b, which confirms quantum confinement with Fabry-Pérot resonances.

On the other hand, this type of nonmonotonic resonance behavior [in $G(V)$; see the black curve in Fig. 2] was recently also reported in another work, and was associated with a Rashba-type spin-orbit coupling in graphene [61]. The $G(V)$ shown in Fig. 2 is identical to those calculated in that work, with the difference that it is the spin, in that work, that is responsible for the effects. This is different from the case of Rashba-type spin-orbit coupling observed in the spin-field effect transistor based on the two-dimensional electron gas (2DEG) of GaAs [62], where the $G(V)$ oscillates differently. In a transistor of GaAs the polarized and opposite conductances oscillate in a sinusoidal way, alternating between them,

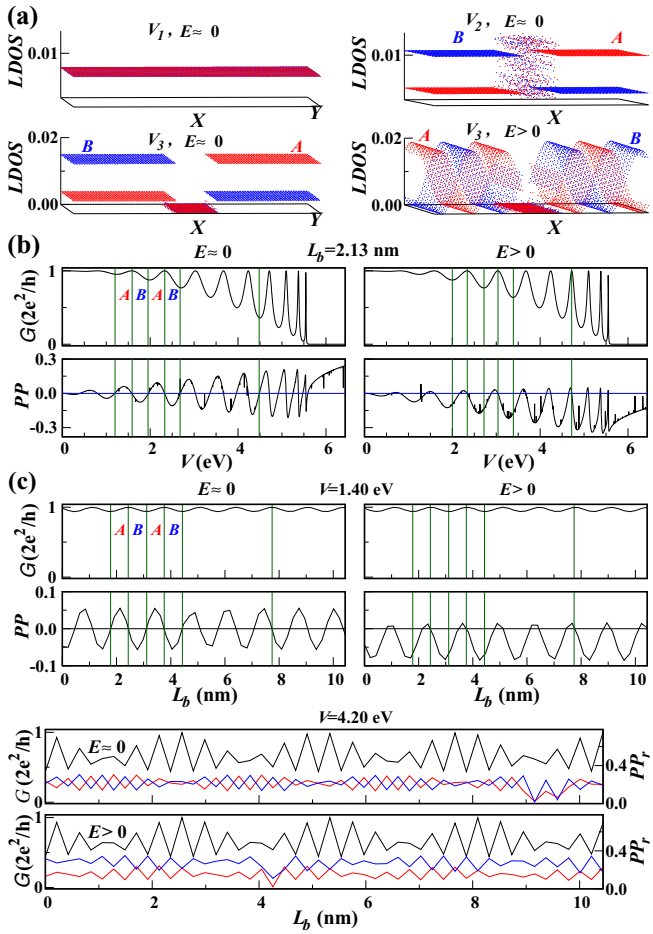

FIG. 3. (a) Typical LDOS for the pure Dirac regime ($V_1 = 0.02$ eV and $E = 0$), for the regime with contributions from the hyperboloid subband ($V_2 = 1.01$ eV and $E = 0$), and for the regime of potential $V_3 = 7.0$ eV of conductance $G = 0$, with $E = 0$ (lack of backscattering) and with $E > 0$ (presence of backscattering). Pseudospintronics is based on the potential V of the applied filter (b) and on the width L_b of the filter (c). For $E > 0$ the PP remains in one sublattice. Different potential V changes the frequency in the $G(L_b)$.

similar to how the PP_r oscillate here in this work, but keeping the frequency. On the other hand, in our work we observe that the PP oscillate between the conductance maximums, this can be deduced by comparing the black curve with the oscillations of the red and blue curves of Fig. 2. Observe here that the conductance maxima are associated with PP = 0, and on the sides of these maxima the PP are opposite. The similarity of the $G(V)$ curves, between our results and those reported in the literature, would require further study in the future.

The transport regimes of the charge carriers, discussed earlier in Fig. 1(b), can be observed here in greater detail in Fig. 2. The pure Dirac regime, even before the resonances of Fabry-Pérot type in the $G(V)$ (for low potential V), has a PP going to zero [see also Fig. 3(a)] for potential V_1 associated with the first regime (pure Dirac regime with $E \approx 0$). This indicates that the contributions PP_r-A and PP_r-B are similar, as shown in Fig. 2. We will find here a perfect match in the interfaces, in relation to the pseudospin orientation. On the other hand, the transmission regime with disturbances from the hyperboloid subband, for medium values of applied V, has typical LDOS (with PP $\neq 0$) of the same type as shown in Fig. 3(a) for the range of potential V_2 associated with the second transport regime [the range of Fabry-Pérot resonances in $G(V)$; black curve in Fig. 2]. We observe in these LDOS the lack of undulations at both sides of the filter; this is associated with the lack of backscattering for $E \approx 0$. Finally, in the last regime a transport gap is generated [see also Fig. 1(b)] for the range of potential V_3. In this case of $G(V_3) = 0$, the PP is frozen in one sublattice, and reaches the maximum value. Here, the states show a total decoupling between the hole-type wave (within the barrier) and the electron-type waves at both sides of the barrier, as shown in Fig. 3(a) for the range of potential V_3 and energy $E \approx 0$. In general, when we move away from the Dirac point ($E > 0$, outside the influence of the pure Dirac regime), undulations (associated with backscattering) at both sides of the filter are observed in all cases; as an example we show Fig. 3(a) for V_3 and $E > 0$. Here the tunneling would be carried out through spatial regions that would have the same type of band; all would be of the hyperboloid subband type for incident particles with high energies, in which case backscattering exists in a natural way.

In Figs. 3(b) and 3(c) we show that a total control of the polarizations PP_A and PP_B (pseudospintronic), can only be obtained around the Dirac point ($E \approx 0$). For $E > 0$ the PP remains frozen in one sublattice; this freezing can be a fingerprint of the emergence of backscattering with increasing energy. For energies (of incident particles) very close to the Dirac point, the PP(V) on the sides of the barrier fluctuates from P-A to P-B in functions of V; for this situation the LDOS on the sides of the barrier have no oscillations. We do not have backscattering associated with normal incidence here. As explained before, we have localization of the state due to the chiral asymmetry localized on the sides of the barrier that increases with V. On the other hand, for energies that move a little away from the Dirac point, we have oscillations of the PP(V) alternating from P-A to zero (or P-B to zero), that is, we have a freezing of the PP(V); for this case also are no observed LDOS oscillations on the sides of the barrier. Finally, for energies well away from the Dirac point, the PP(V) cannot be better defined and only the value of zero is observed; here undulations (from LDOS) on the sides of the barrier are observed, associated with backscattering. In this way, the intermediate regime [with PP(V) freezing] would be associated with the transition between the absence and the presence of backscattering for normal incidence in the barrier.

Also, the line forms observed in the G remain unchanged as a function of V [see (b)], and also as a function of L_b [see (c)], for all energies close to the Dirac point. Both in (b) and in (c), around the Dirac point ($E \approx 0$), it is observed that the maxima and minima of G are associated with PP = 0; between these maxima and minima, the maximum PP are observed. Here, in the intervals between the maxima and minima of the $G(V)$, it is observed that the LDOS have the typical form as shown in Fig. 1(d), from which it can be intuited that a wave type A (or B) enters and a wave type B (or A) leaves; that is, at both sides of the filter the pseudospins have a phase difference of π at those intervals. The periodically uniform behavior of the conductance $G(L_b)$, observed in (c) for $E \approx 0$, is analogous

to that reported in graphene systems with Rashba spin-orbit interaction [61]. Here, the frequencies observed in the conductance $G(L_b)$, discussed above, for different potentials V of the filter, are associated with the PP_A and PP_B, as shown in the figure. In general, in all cases, we observe the inverse relationship between the G and PP, as well as the freezing of PP for $E > 0$.

On the other hand, an interesting application of the tunability of the anti-Klein tunneling induced by the filters of pseudospin is related to a technique that provides modulatable gaps in the conductance, i.e., we can manipulate the semiconductor properties of the graphene nanoribbon. In Fig. 4(a), we show the results obtained with a mixed filter (top), i.e., an effective potential that is obtained by applying simultaneously a potential V and a potential $V_1 = -V - \delta V$, with V always positive. In this figure, we can see an increase of the partial pseudospin polarization PP(V) with the application of the mixed filter. Also, we suppress the freezing of the PP inversion away from the Dirac point, favoring in this way polarizations that can be inverted for a greater energy interval. The PP(V) increases as we increase the difference δV between the applied potentials, which leads to an increase in the depth of the minima in $G(V)$ and the subsequent formation of transport gaps.

The most important results about the appearance of adjustable gaps for high applied voltages V are shown in Fig. 4(b). In those maps $[G(V, E)]$, the gaps appear more clearly as we increase V. Note that there are regions in which the gap can be increased or decreased. In general, a periodic modulation as a function of V is obtained. The difference between the potentials V and V_1 generates displacements in the gaps' energy and also they are tilted in relation with the vertical axis E. When the absolute value of V_1 is greater than the potential V, the gaps are tilted to the left, and when the potential V is greater than $|V_1|$, the gaps are tilted to the right. Therefore, the application of the potential V (V_1) displaces the lower (upper) hyperboloid subbands for the Dirac point, as will be explained later. The symmetric contributions of the hyperboloid subbands (lower and upper) generate the symmetric gaps around the Dirac point, as shown by the configuration $/V/V_1 = -V/$. This will be discussed in the following figure.

In Fig. 4(c), we use $V_1 = -V$ and study effective potentials of the type $/V/V_1/V/V_1/V/V_1/\cdots$, with n filters applied. The filter V raises the lower hyperboloid subbands (found below the Dirac point) and the $V_1 = -V$ filter lowers the upper hyperboloid subbands (found above the Dirac point), all contributing near the Dirac point. Here, n odd means an asymmetric contribution between the upper and lower hyperboloid subbands (column on the left). On the other hand, n even means that the upper and lower hyperboloid subbands contribute symmetrically to the Dirac point (column on the right). The asymmetric system (n odd) shows in the maps of $G(V, E)$ also an asymmetry, here we see asymmetric forms in the gaps and intensities of G below a quantum of conductance (orange regions on the map). On the other hand, the symmetric system (n even) shows a decrease of the orange regions (G increase) and it is also observed that the shapes of the gaps on the map are symmetrical. In general, with the increase of n we can better define the gaps, that is, we see a better definition of the black regions on the map. An interesting and unexpected

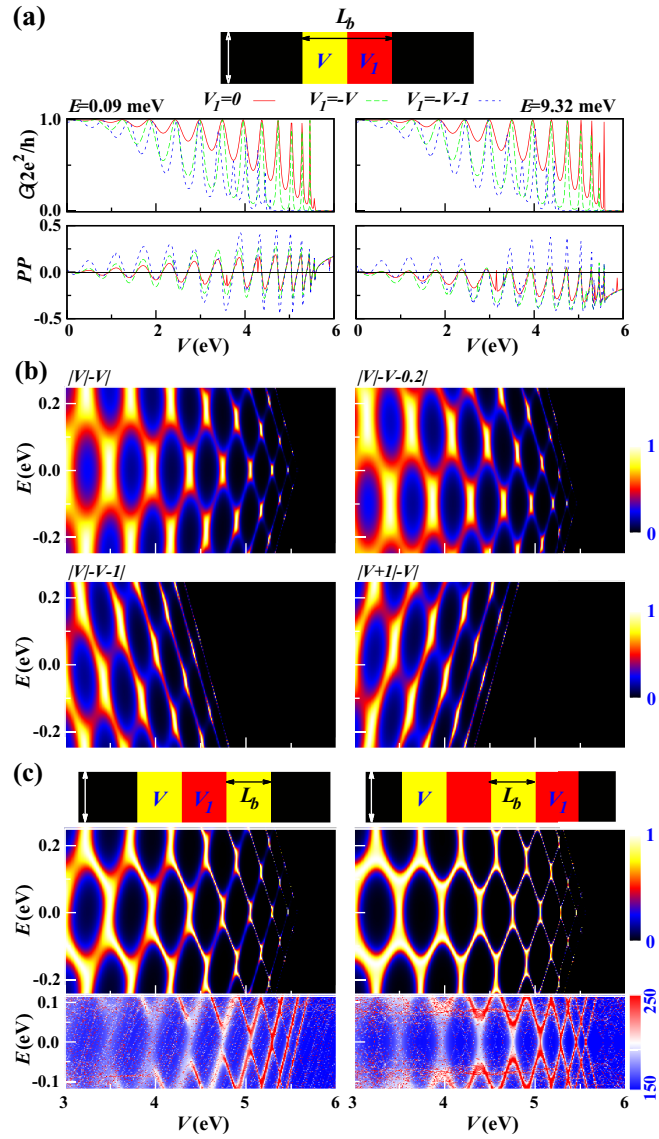

FIG. 4. (a) Conductance and partial pseudospin polarization based on V for the mixed filter ($/V/V_1/$) shown in the inset. (b) Conductance maps for different configurations of $/V/V_1/$, showing the manipulation of the induced gaps. (c) $G(V, E)$ for the mixed filter with $n = 3$ (asymmetric) and with $n = 4$ (symmetric). At the bottom we have DOS(V, E) maps, showing the contribution of the hyperboloid subbands (lower and upper) for the Dirac point.

result is that the asymmetric and symmetric contributions of the hyperboloid subbands seem to be mapped in DOS(V, E) maps; see the lower panels of Fig. 4(c). In these maps, we observe that the upper and lower hyperboloid subbands (red curves) are closer and closer to the Dirac point with the increase of V, and that these contributions are symmetric for n even (right panel), differently from what is observed in the left panel for the asymmetric system (n odd). Later, we will further discuss these DOS(V, E) maps.

In the following, in Fig. 5, we will discuss how to optimize the technique of inducing controllable gaps, to encourage experimental work. We will also test here the robustness of our results in relation to the imperfections of the system and we

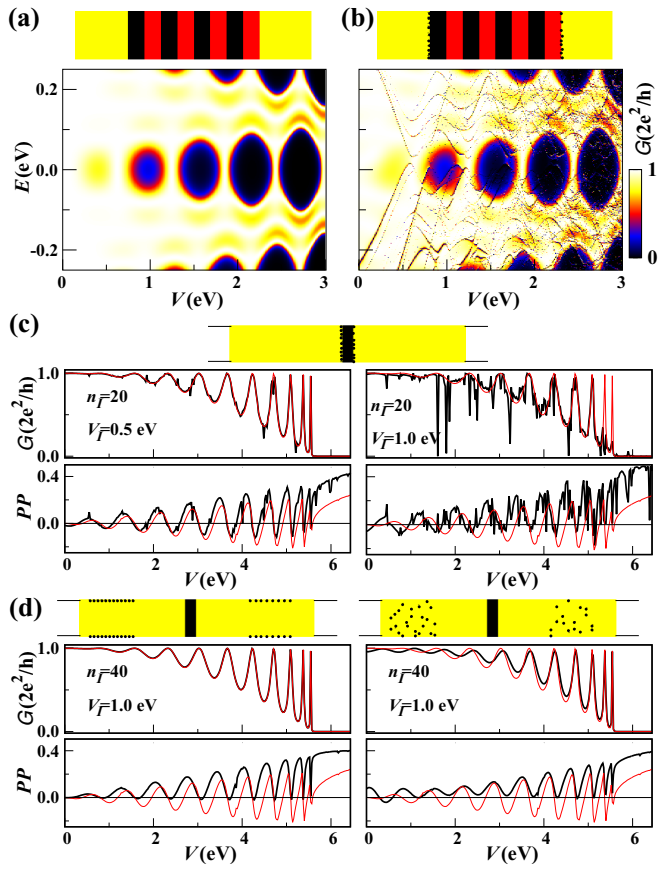

FIG. 5. (a) By increasing the number of filters ($n = 8$) of the mixed filter, we can induce gaps for low potential V. (b) Roughness at the ends of the mixed filter induces a recovery of the Klein tunneling in the gap regions. (c) The increase in the intensity of the potential V_I of the roughness, maintaining the number of roughness n_I, destroys the nonmonotonic behavior. (d) The nonmonotonic behavior is robust against imperfections in the borders and bulk of the nanoribbon.

will study the recovery of Klein's tunneling associated with these imperfections. In (a) we show that for $n = 8$ we can induce controllable gaps for low potentials V. In general, the increase of n improves the definition of gaps, which from the experimental point of view is important. With an appropriate n we can adjust an interval of V for a specific need. In (b), with the inclusion of roughness at the ends of the effective barrier, we observe a recovery of the Klein tunneling in the gap regions. This effect of suppressing Klein's antitunneling using disorder is analogous to that observed in bilayer graphene p-n junction, here induced now in graphene monolayers (nanoribbons). This implies that, under certain circumstances, a revival of the Klein tunneling in monolayers graphene is possible, by manipulating the gap-controlled Berry phase. Also, in monolayer graphene (nanoribbons), signatures of the broken chirality due to band gap opening should appear in the Berry phase, which varies as a function of the induced asymmetry (roughness) and might be accessible in the Fabry-Pérot resonances, [28] found in $G(V)$.

To understand the role of the disorder (roughness on the sides of the effective barrier) on the Fabry-Pérot resonances, and the relationship with the loss of chirality discussed above, we use parts (c) and (d), where to simplify we use $n = 1$, and so we can also complement Figs. 2 and 3. Here, we use a phenomenological model of imperfections, and we fix the number of perturbed sites or impurities (n_I) and their potentials (V_I), with the positions of impurities randomly distributed. Then, we study several configurations. The values used for n_I and V_I are in Figs. 5(c) and 5(d). As discussed before, the filter-nanoribbon interfaces are the regions where the coupling of the pseudospin (of the electron-type waves on the sides of the filter) occurs with the hole-type wave (inside the filter). In Fig. 5(c), we observe that the coupling is damaged by fluctuations and freezing of the PP(V) at both sides of the filter, caused by asymmetry in the interfaces when we increase the intensity V_I of the roughness. This leads to a gradual destruction of the Fabry-Pérot resonances [detected in $G(V)$] as we increase the asymmetry in the filter. Here, similarly to what happens in bilayer graphene p-n junction, the Berry phase [accordingly PP(V)] also depends on the asymmetry (roughness in the filter). We observe in panel (c) an difference in phase in the PP(V), between the black (with roughness) and red (without roughness) curves, which increases when we increase the asymmetry, which is directly associated with freezing of PP. Note that for disturbed cases (black curve) the PP(V) is not zero for the maxima (and minima) of the $G(V)$ for high values of V_I. In general, with the increase of V_I, the conductance $G(V)$ associated with the loss of chirality shows strong localizations (dips) with frozen of the PP; generally, we have a destruction of the Fabry-Pérot resonances, which does not characterize the conservation of chiral symmetry of the state.

On the other hand, imperfections on the borders of the nanoribbon and also within the bulk [panel (d)] do not generate localizations (dips), showing only the freezing of the PP, that is, that type of imperfections alters less the electron-hole coupling of state, when compared with the roughness at the ends of the filter. Also in Fig. 5(d), a system with imperfections (asymmetry) in the edges and bulk of the nanoribbon, the chiral symmetry of the state is conserved. With the increase of the asymmetry (imperfections), the system, to preserve the chiral symmetry of the state, increases the asymmetry on the sides of the barrier, that is, the PP goes from a pseudospin oscillation regime (A to B) to a regimen where a type of pseudospin (A or B) is conserved, here called freezing. This last regime includes the increase of asymmetry caused by the increase of imperfections. Thus, before the state loses chiral symmetry, the PP freezes, as a sign of the increase in asymmetry before backscattering is generated. In general, the system evolves, increasing the local asymmetry (PP) and preserving the chirality of the state, as imperfections increase. This is an example of how the chiral symmetry can evolve and still be conserved.

In Fig. 6, we discuss a technique to qualitatively map the contributions of the hyperboloid subbands to the Dirac point, using DOS(V, E) maps. This procedure shows how the hyperboloid subbands evolve because of the applied filter, as the potential V increases. In (a), we observe that those effects cannot be mapped when a single filter is used ($+V$ or $-V$). On the other hand, the use of two filters to form an effective filter of $/+V/-V/$ type [see inset of the Fig. 4(a)] allows

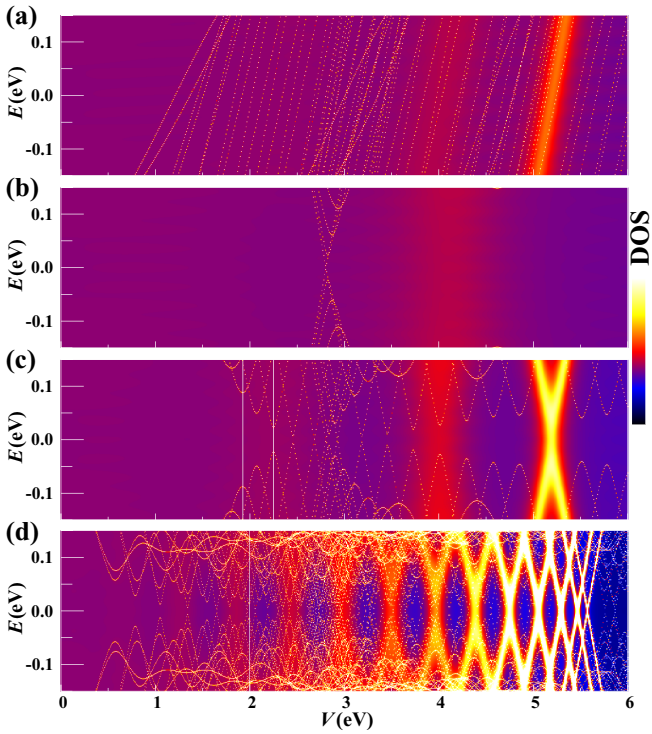

FIG. 6. Mapping of electronic bands $E(V)$ and the effects associated with the loss of the chirality property on DOS(V, E) maps, using pseudospin filters. (a) Using a single filter we cannot perform the mapping ($L_b = 4$ sites). (b) The use of a mixed filter of the type $/+V/-V/$ allows mapping (with $L_b = 4$ sites per filter). By increasing the width L_b of each filter, the mapping is optimized and induced for low potential V. (c) $L_b = 8$ sites and (d) $L_b = 14$ sites.

mapping the contributions of the hyperboloid subbands [(b), (c), and (d)].

The DOS(V, E) maps shown in Figs. 6(b), 6(c), and 6(d) map the energy bottom (conduction) and energy top (valence) of the hyperboloid subbands (closer to the Dirac point) arriving at the Dirac point; this is done following the behavior of the van Hove singularities (which are found where a hyperboloid subband begins). These van Hove singularities on the maps are the most intense points of light color. For reference, look at the two vertical lines in Fig. 6(c) [which would be DOS(E) for different V]. Where the straight lines intersect the curves on the map are the van Hove singularities. In these maps we can see how the system energies change as a function of V. These maps show the disturbed energies $E(V)$. On the other hand, these maps allow us to see that the hyperboloid subbands (seen here as van Hove singularities: Bottom and top of the hyperboloid subbands closest to the Dirac point) arrive at the Dirac point, touch, and then move away from it. Interestingly, before they touch, the mapped format is parabolic and, when they touch at $E = 0$, the mapped format is linear, reminiscent of hyperboloid subbands and Dirac bands respectively. On the other hand, it is known that, in materials called topological isolators, when the parabolic bands (conduction and valence) are pushed in order to touch, for example by pressure on the material, the bands are linearized when they touch, forming a format of Dirac bands. Also, in general, around the Dirac point [where the $E(k)$ bands are linear] it is known that the DOS is proportional to the energy E. All this is indicating that the $E(V)$ mapped (close to the Dirac point) from the DOS would be including the information of the $E(k)$ disturbed by V.

Even if the contributions of the hyperboloid subbands to the Dirac point are symmetrical for this effective filter ($n = 2$), we observe an asymmetry of the bands in relation to the horizontal axis. Also in this figure [panel (b)], we observe that for low applied potentials V the mapping effect is not induced. On the other hand, the increase in the width L_b of the filters ($+V$ and $-V$) allows the increase the intensity of the contributions of the hyperboloid subbands, and also induces such contributions for lower applied potential V [see (c) and (d)], as also observed in Fig. 2.

The main effects on the mapped bands $E(V)$, depending on the applied potential V, are shown in panels (c) and (d). In (c), for example, we can observe some electronic transport regimes that can be well differentiated. For low V, we do not have mapped bands $E(V)$, which indicates a pure Dirac regime. With the increase of V, the bands are observed, especially as the hyperboloid subbands are getting closer and closer to the Dirac point, to contribute to electronic transport. Subsequently, for higher potentials V the bands are repelled, that is, the formation of a transport gap is observed (a known effect in the literature from the loss of chirality), until resonant tunneling states are formed with the increase of V [associated with the fine peaks observed in the $G(V)$ for high potentials, discussed earlier in Figs. 2 and 3]. This last transport regime is associated with the thick yellow lines observed in the DOS(V, E) maps, which resemble Dirac's bands (cones). Finally, we have a total localization of the states, shown on the maps; everything that follows after the thick lines (cones) disappears.

All these effects can be carried for lower potential V, as shown in (d), by increasing the width L_b of the filter, which is very important from the experimental point of view; that is, we can induce these effects for low potentials. This technique proposed here in this work to map the bands $E(V)$ results in an interesting tool for theoretical and experimental investigations.

On the other hand, it is interesting to discuss here the suspicion of a possible pseudospin-orbit interaction in our system, which could occur for large values of the width L_b of the applied filter. The spin-orbit interaction present in two-dimensional electron gas systems is due to the lack of spatial symmetry [63–66]; as a consequence, the spin degeneracy in k-space is lifted, which is known as Rashba splitting. It induces a spin precession in the carriers moving in the gas (detected in conductance as oscillations), and the strength of this spin-orbit interaction can be tuned using an electric field perpendicular to the gas [62]. These spin effects are also observed in the transport of charge through graphene-based systems.

It is interesting to observe a possible effect related to the Rashba pseudospin-orbit split in the second and third mappings of the Fig. 6(d) (between 0.7 and 1.3 eV), for the bands closest to Dirac's point. We observe here that, in the second mapping, the second band is dislocated to the right, and, on the other hand, the second band in the third mapping is dislocated to the left. This effect could be related to the

decoupled branches of opposite pseudospin [66], which is in evidence before $V = 1.5$ eV, where these subbands meet, before the formation of the energy gap.

In general, the $G(V)$ in our work already has a pseudospin-orbit coupling fingerprint, because it is identical with the $G(V)$ observed in the literature, with respect to its spin-orbit coupling analog [61]. Here we reinforce this suspicion, mapping the energy bands $E(V)$, where other fingerprints are observed, such as the Rashba pseudospin-orbit split (decoupled branches of opposite pseudospin) [62–64,66]. In these maps the different known characteristics of the Rashba effect seem to be a function of the strength of this pseudospin-orbit interaction (potential of filter, V) for filters with large widths L_b. In general, all these suspicions can only be verified if we use a model Hamiltonian to support this analogy; this could be part of future research.

In the Figs. 1(c) and 6 we show that hyperboloid subbands can reach the Dirac point ($E = 0$) for high potentials V of the applied barrier, consequently the Dirac band will be disturbed in the barrier region. This changes the characteristics of the bands within the barrier region and causes the effects seen in Fig. 2. In general, the tunneling observed in Fig. 2 occurs through regions that contain different types of bands (not all of the pure Dirac type); for this reason the nanoribbon-barrier interfaces control the tunneling. These interfaces control electron-hole coupling, which is decreasing with increasing V, due to chiral asymmetry in those regions (on the sides of the barrier). The displacement of the hyperboloid subbands for the Dirac point is evident in Figs. 6(c) and 6(d), where clearly the van Hove singularities of the DOS (which are found where a hyperboloid subband begins) approach each other again for the point $E = 0$ as V increases.

IV. CONCLUSION

We have shown here in this work that a gradual and controlled loss of chirality can be induced in graphene nanoribbons using pseudospin filters. These filters generate contributions from the hyperboloid subbands for regions near the Dirac point. As a consequence, opposite polarizations of pseudospin are generated at both sides of the applied filter, which creates a spatial asymmetry. This asymmetry disfavors the coupling of the pseudospin at both sides of the filter with the hole-type wave inside the filter, as a function of the potential of the applied filter.

The oscillations observed in the conductance as a function of the potential of the applied filter, are related to Fabri-Pérot resonances with frequencies that depend on the applied potential. In this way, a gradual evolution of Klein antitunneling is observed, with the final generation of an transport gap. Using specific configurations of the applied filters, we can manipulate the induced energy gaps to have better control that can be tested experimentally. The Klein tunneling can be recovered by the introduction of another type of asymmetry, for example, roughness on the edges of the applied filters; this effect is similar to that observed in bilayer graphene p-n junction.

We also show here that pseudospin filters can be used to map the energy bands $E(V)$ [on DOS(V, E) maps], which allows the gradual observation of the effects produced in the energies caused by external disturbances. Here, in this work, we observe in the bands $E(V)$ the different effects caused by the contributions of the hyperboloid subbands. This technique proposed here results in an experimental and theoretical tool capable of complementing different studies based on graphene systems; it is also possible to be able to extrapolate for systems that have the property of pseudospin.

In general, the increase in V carries the hyperboloid subbands to the Dirac point; this leads to a transition from a Dirac type regime to a disturbed Dirac-type regime, with a gradual loss of chiral correlations as a function of V. This transition depends on the width L_b of the applied barrier. The transition is observed as a periodic loss of the chirality property (correlation between pseudospins), consequently we have a gradual loss of coupling between the electron-type wave on the sides of the barrier with the hole-type wave inside the barrier. This is observed as a decrease in the line width of the resonances in $G(V)$ as V increases. This can be interpreted as a decoupling between the pseudospin on the sides, with the wave confined in the barrier. The fingerprint of this transition in the $G(V)$ would be the nonmonotonic behavior; here the minima of $G(V)$ would be associated with the evolution of the gap as a function of V. Interestingly, throughout the tunneling process with local pseudospin oscillations, the chiral symmetry of the state is preserved. This is an example of how the chiral symmetry can evolve and still be conserved, during a tunneling process.

Transmission oscillations with a nonmonotonic behavior were also recently reported (through a barrier with potential energy V), as a product of a spin-orbit coupling of Rashba type, in graphene monolayers [61]. The line form of the conductance $G(V)$, found in that paper, is identical to that observed in our work, which raises a suspicion about a possible Rashba pseudospin-orbit interaction in our work. That reference notes a decrease in the resonance line width as a function of V to finally form a transport gap. The appearance of a gap due to spin-orbit coupling in graphene is a fingerprint of this coupling [67–70]. The latter reference is interesting because it exploits the chirality of the low-energy states to resolve this gap.

In this way the nonmonotonic behavior of the conductance $G(V)$ for large widths L_b (Fig. 2) and the effects observed in the mapping of the bands $E(V)$ [Fig. 6(d)] show evidence of possible pseudospin-orbit coupling in our system. In general, the manipulation of the coupling between the pseudospin inversions observed on the sides of the barrier, with the wave confined within the barrier, could generate a Rashba pseudospin-orbit coupling as a function of V. The asymmetry caused by the polarization PP on the sides of the barrier could favor the Rashba effect. Suspicions regarding the Rashba effect are not conclusive and further work on this matter is needed in the future.

Finally, the studies carried out here in this work show that the pseudospin has an important effect, capable of being able

to compete with the effects of spin, as shown by the similarity between the conductances reported here with the conductances associated with Rashba-type spin-orbit coupling. In this way it would be necessary in the future to pursue a deeper study of the competition between the pseudospin and the spin.

ACKNOWLEDGMENTS

The authors acknowledge financial support from Universidade Federal do ABC, Universidade Federal do Sul e Sudeste do Pará, and Brazilian agency FAPESP.

[1] M. Elbistan, C. Duval, P. A. Horvathy, and P. M. Zhang, Phys. Lett. A **380**, 1677 (2016).
[2] A. K. Geim and K. S. Novoselov, Nat. Mater. **6**, 183 (2007).
[3] L. Majidi and M. Zareyan, Phys. Rev. B **83**, 115422 (2011).
[4] R. Decker, Y. Wang, V. W. Brar, W. Regan, H. Z. Tsai, Q. Wu, W. Gannett, A. Zettl, and M. F. Crommie, Nano Lett. **11**, 2291 (2011).
[5] M. B. Lundeberg and J. A. Folk, Science **346**, 422 (2014).
[6] Y. Tang and A. E. Cohen, Phys. Rev. Lett. **104**, 163901 (2010).
[7] L. D. Barron, *Molecular Light Scattering and Optical Activity* (Cambridge University Press, Cambridge, 2009).
[8] M. B. Smith and J. March, *March's Advanced Organic Chemistry: Reactions, Mechanisms and Structure* (Wiley, New York, 2007).
[9] Y. Inoue and V. Ramamurthy, *Chiral Photochemistry* (Marcel Dekker, New York, 2004).
[10] B. Göhler, V. Hamelbeck, T. Z. Markus, M. Kettner, G. F. Hanne, Z. Vager, R. Naaman, and H. Zacharias, Science **331**, 894 (2011).
[11] W. F. Koehl, M. H. Wong, C. Poblenz, B. Swenson, U. K. Mishra, J. S. Speck, and D. D. Awschalom, Appl. Phys. Lett. **95**, 072110 (2009).
[12] C. J. Kim, A. S. Castillo, Z. Ziegler, Y. Ogawa, C. Noguez, and J. Park, Nat. Nanotechnol. **11**, 520 (2016).
[13] J. R. Wallbank, D. Ghazaryan, A. Misra, Y. Cao, J. S. Tu, B. A. Piot, M. Potemski, S. Pezzini, S. Wiedmann, U. Zeitler, T. L. M. Lane, S. V. Morozov, M. T. Greenaway, L. Eaves, A. K. Geim, V. I. Fal'ko, K. S. Novoselov, and A. Mishchenko, Science **353**, 575 (2016).
[14] A. H. Castro Neto, F. Guinea, N. M. R. Peres, K. S. Novoselov, and A. K. Geim, Rev. Mod. Phys. **81**, 109 (2009).
[15] S. Y. Zhou, G. H. Gweon, J. Graf, A. V. Fedorov, C. D. Spataru, R. D. Diehl, Y. Kopelevich, D. H. Lee, S. G. Louie, and A. Lanzara, Nat. Phys. **2**, 595 (2006).
[16] A. Bostwick, T. Ohta, T. Seyller, K. Horn, and E. Rotenberg, Nat. Phys. **3**, 36 (2007).
[17] M. Mucha-Kruczyński, O. Tsyplyatyev, A. Grishin, E. McCann, V. I. Fal'ko, A. Bostwick, and E. Rotenberg, Phys. Rev. B **77**, 195403 (2008).
[18] M. I. Katsnelson, K. S. Novoselov, and A. K. Geim, Nat. Phys. **2**, 620 (2006).
[19] M. I. Katsnelson, Eur. Phys. J. B **51**, 157 (2006).
[20] A. F. Young and P. Kim, Nat. Phys. **5**, 222 (2009).
[21] O. Klein, Z. Phys. **53**, 157 (1929).
[22] J. R. Williams, L. DiCarlo, and C. M. Marcus, Science **317**, 638 (2007).
[23] E. McCann and V. I. Fal'ko, Phys. Rev. Lett. **96**, 086805 (2006).
[24] E. McCann, Phys. Rev. B **74**, 161403(R) (2006).
[25] E. McCann, D. Abergel and V. Fal'ko, Solid State Commun. **143**, 110 (2007).
[26] M. M. Kruczyński, E. McCann, and V. I. Fal'ko, Solid State Commun. **149**, 1111 (2009).
[27] R. Du, M. H. Liu, J. Mohrmann, F. Wu, R. Krupke, H. von Löhneysen, K. Richter, and R. Danneau, Phys. Rev. Lett. **121**, 127706 (2018).
[28] A. Varlet, M. H. Liu, D. Bischoff, P. Simonet, T. Taniguchi, K. Watanabe, K. Richter, T. Ihn, and K. Ensslin, Phys. Status Solidi RRL **10**, 46 (2016).
[29] A. Varlet, M. H. Liu, V. Krueckl, D. Bischoff, P. Simonet, K. Watanabe, T. Taniguchi, K. Richter, K. Ensslin, and T. Ihn, Phys. Rev. Lett. **113**, 116601 (2014).
[30] P. Rickhaus, R. Maurand, M. H. Liu, M. Weiss, K. Richter, and C. Schönenberger, Nat. Commun. **4**, 2342 (2013).
[31] M. V. Berry, Proc. R. Soc. Lond. A **392**, 45 (1984).
[32] S. Pancharatnam, Proc. Ind. Acad. Sci. A **44**, 247 (1956).
[33] Y. Aharonov and D. Bohm, Phys. Rev. **115**, 485 (1959).
[34] S. J. Choi, S. Park, and H. S. Sim, Phys. Rev. B **89**, 155412 (2014).
[35] C. Dutreix, H. G. Herrero, I. Brihuega, M. I. Katsnelson, C. Chapelier, and V. T. Renard, Nature (London) **574**, 219 (2019).
[36] K. Novoselov, A. K. Geim, S. Morozov, D. Jiang, M. K. I. Grigorieva, S. Dubonos, and A. Firsov, Nature (London) **438**, 197 (2005).
[37] Y. Zhang, Y. W. Tan, H. L. Stormer, and P. Kim, Nature (London) **438**, 201 (2005).
[38] S. Park and H. S. Sim, Phys. Rev. B **84**, 235432 (2011).
[39] E. McCann and M. Koshino, Rep. Prog. Phys. **76**, 056503 (2013).
[40] K. Sasaki, K. Wakabayashi, and T. Enoki, New J. Phys. **12**, 083023 (2010).
[41] S. R. E. Yang, Nanomaterials **9**, 885 (2019).
[42] K. I. Sasaki, K. Kato, Y. Tokura, K. Oguri, and T. Sogawa, Phys. Rev. B **84**, 085458 (2011).
[43] L. I. A. López, S. M. Yaro, A. Champi, S. Ujevic, and M. Mendoza, J. Phys.: Condens. Matter **26**, 065301 (2014).
[44] L. I. A. López, A. Champi, S. Ujevic, and M. Mendoza, Eur. Phys. J. B **88**, 298 (2015).
[45] L. I. A. López, S. Ujevic, and M. Mendoza, J. Phys. Commun. **2**, 035020 (2018).
[46] L. I. A. López and M. Mendoza, Eur. Phys. J. B **91**, 157 (2018).
[47] L. I. A. López, S. Ujevic, and M. Mendoza, J. Phys.: Condens. Matter **31**, 155303 (2019).
[48] S. De Leo and P. Rotelli, Int. J. Theor. Phys. **37**, 2193 (1998).
[49] E. Serna, I. R. Vargas, R. P. Álvarez, and L. D. Cisneros, J. Appl. Phys. **125**, 203902 (2019).
[50] M. J. Majid and M. H. Alaa, J. Kufa Phys. **10**, 31 (2018).
[51] Y. W. Son, M. L. Cohen, and S. G. Louie, Phys. Rev. Lett. **97**, 216803 (2006).
[52] D. K. Ferry and S. M. Goodnick, *Transport in Nanostructures* (Cambridge University Press, Cambridge, 1997).

[53] K. Wakabayashi, M. Fujita, H. Ajiki, and M. Sigrist, Phys. Rev. B **59**, 8271 (1999).
[54] A. V. Rozhkov, S. Savel'ev, and F. Nori, Phys. Rev. B **79**, 125420 (2009).
[55] S. Datta, *Electronic Transport in Mesoscopic Systems* (Cambridge University Press, New York, 1995).
[56] M. Mendoza and S. Ujevic, J. Phys.: Condens. Matter **24**, 235302 (2012).
[57] M. Mendoza and P. A. Schulz, Phys. Rev. B **68**, 205302 (2003).
[58] D. S. Fisher and P. A. Lee, Phys. Rev. B **23**, 6851(R) (1981).
[59] H. Zheng, Z. F. Wang, T. Luo, Q. W. Shi, and J. Chen, Phys. Rev. B **75**, 165414 (2007).
[60] S. Reich, J. Maultzsch, C. Thomsen, and P. Ordejon, Phys. Rev. B **66**, 035412 (2002).
[61] L. Dell'Anna, P. Majari, and M. R. Setare, J. Phys.: Condens. Matter **30**, 415301 (2018).
[62] F. Mireles and G. Kirczenow, Phys. Rev. B **64**, 024426 (2001).
[63] E. A. de Andrada e Silva, G. C. La Rocca, and F. Bassani, Phys. Rev. B **55**, 16293 (1997).
[64] A. Soumyanarayanan, N. Reyren, A. Fert, and C. Panagopoulos, Nature (London) **539**, 509 (2016).
[65] E. G. Mishchenko and B. I. Halperin, Phys. Rev. B **68**, 045317 (2003).
[66] M. Gmitra, S. Konschuh, C. Ertler, C. Ambrosch-Draxl, and J. Fabian, Phys. Rev. B **80**, 235431 (2009).
[67] Y. Yao, F. Ye, X. L. Qi, S. C. Zhang, and Z. Fang, Phys. Rev. B **75**, 041401(R) (2007).
[68] B. Berche, F. Mireles, and E. Medina, Condens. Matter Phys. **20**, 13702 (2017).
[69] B. Yang, M. F. Tu, J. Kim, Y. Wu, H. Wang, J. Alicea, R. Wu, M. Bockrath, and J. Shi, 2D Mater. B **3**, 031012 (2016).
[70] J. Sichau, M. Prada, T. Anlauf, T. J. Lyon, B. Bosnjak, L. Tiemann, and R. H. Blick, Phys. Rev. Lett. **122**, 046403 (2019).